JACS
JOURNAL OF THE AMERICAN CHEMICAL SOCIETY

Article

pubs.acs.org/JACS

Reversible Solid-to-Liquid Phase Transition of Coordination Polymer Crystals

Daiki Umeyama,[†] Satoshi Horike,*[,†,‡] Munehiro Inukai,[§] Tomoya Itakura,[∥] and Susumu Kitagawa*[,†,§]

[†]Department of Synthetic Chemistry and Biological Chemistry, Graduate School of Engineering, Kyoto University, Katsura, Nishikyo-ku, Kyoto 615-8510, Japan

[‡]PRESTO, Japan Science and Technology Agency, 4-1-8 Honcho, Kawaguchi, Saitama 332-0012, Japan

[§]Institute for Integrated Cell-Material Sciences (WPI-iCeMS), Kyoto University, Yoshida, Sakyo-ku, Kyoto 606-8501, Japan

[∥]DENSO Corporation, 1-1 Showa-cho, Kariya, Aichi 448-8661, Japan

Supporting Information

ABSTRACT: The solid-to-liquid phase transition, a fundamental process commonly observed for various types of substances with significant potential for application, has been given little attention in the field of coordination polymers (CPs) despite the rich functionality of these compounds. In this article, we report the reversible solid-to-liquid phase transition of crystalline CPs. These CPs are composed of zinc ions, phosphate, and azoles, and a well-balanced composition, ionicity, and bond strength afford "melting" CPs. We examined the structure of one such melting framework in the liquid and glass states and found that the coordination bonds are not fully preserved in the liquid state but are reformed in the glass state. As a demonstration, we fabricated, via phase transition, a thin film with an aligned crystal orientation and a monolith crystal of the CP.

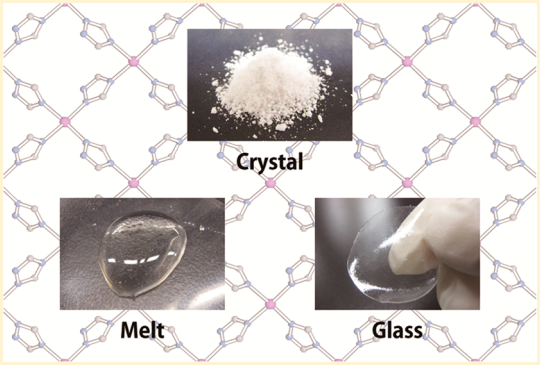

INTRODUCTION

The phase transition from solid to liquid is one of the most fundamental and important phenomena in materials science.[1] This phenomenon offers beneficial processability and formability for functional solid-state materials through a process known as "melt growth."[2] For example, giant single crystals of Si (a semiconductor element) and $LiNbO_3$ (a ferroelectric material) can be grown from their liquid states; the resulting materials thus function as desired when integrated into devices.[3] It is also feasible to fabricate glasses via this phase transition, which has vital importance for optical applications.[4]

The melting of substances is a process during which cohesive forces working in solids "loosen" at a certain temperature. In the cases of the melting of small molecules, macromolecules (polymers), metals, and salts, the cohesive forces such as van der Waals forces, hydrogen bonds, metallic bonds, and ionic bonds loosen to turn into fluid liquids.[5] The melting of the solids that have covalent bonds as cohesive forces is relatively limited; crystalline silicon and quartz are the examples of covalently extended melting solids. When it comes to inorganic–organic hybrid materials (hybrid nanocomposites in molecular scale),[6] in which a variety of cohesive forces may coexist, the melting phenomena are rarely known. Although inorganic–organic hybrid materials occupy an important position for materials scientists, the reversible solid-to-liquid phase transition of these hybrid materials have not been explored, thus being a missing discipline in materials science.

Coordination polymers (CPs) are a class of crystalline inorganic–organic hybrids that form extended networks via coordination bonds, which are the main cohesive forces of these materials.[7] CPs exhibit interesting properties in magnetism,[8] photonics,[9] electronic and ionic conductions,[10] and CPs with open structures, so-called porous coordination polymers (PCPs) or metal–organic frameworks (MOFs), demonstrate a wider functionality including gas storage/separation and heterogeneous catalysis.[11] While a large body of research on the synthesis of CPs has been reported, the melting of CPs is not widely observed because most CPs decompose irreversibly when heated, with a few exceptions.[12] Therefore, exploring the solid–liquid phase transition of CPs in a systematic way is important for the better functionalization of CPs[13] (via melt growth, glass formation, and shaping ability) as well as to developing a melting system in inorganic–organic hybrid chemistry. In particular, how the main cohesive forces, coordination bonds, are loosened or preserved before and after the melting and glass-forming processes of CPs is of fundamental interest, on the analogy of covalent organic polymers.

In this study, we report in detail the synthesis of a series of melting CPs, the melting process mechanism, the structure of molten CPs, and the application of the melting behavior for a

Received: October 27, 2014
Published: December 19, 2014

DOI: 10.1021/ja511019u
J. Am. Chem. Soc. 2015, 137, 864–870

comprehensive study of melting CPs. By using ionic components, we have found a qualitative design guide for melting frameworks. This study exploits a new research area for crystalline inorganic–organic hybrid materials and will lead to a useful strategy for both the synthesis and processing of hybrid materials (potentially including PCPs/MOFs) by introducing the concept of phase diagram to inorganic–organic hybrid chemistry.

RESULTS AND DISCUSSION

In this report, we define "melting" for CPs as a reversible transformation process from solid to liquid, and six CPs will be discussed in terms of melting. The first compound, a proton-conductive CP, $[Zn(HPO_4)(H_2PO_4)_2]\cdot 2H_2Im$ (**1**; Im: imidazolate),[12a] exhibits a reversible solid–liquid phase transition as shown in Figure 1. We denote the crystalline (solid) state as **1**, the molten (liquid) state as **1′**, and the glassy (supercooled) state as **1″**. Five more structures are examined in terms of melting for comparison: $[Zn(H_2PO_4)_2(HTr)_2]$ (**2**; Tr: 1,2,4-triazolate),[14] $[Zn_3(H_2PO_4)_6(H_2O)_3]\cdot HBim$ (**3**; Bim: benzimidazolate)[15] and the frameworks analogous to **3** (**4**, **5**, and **6**). These compounds consist of phosphates and azoles as ligands that bridge the metal ions to form extended coordination structures. The crystal structures of **1** and **2** are shown in Figure 2. The extended networks are formed via bridging phosphates for **1** and bridging 1,2,4-triazole for **2**; thus, each ligand presents cohesive forces in the structures. Table S1 in Supporting Information summarizes the thermal behaviors of the series of CPs that will be discussed here. For all the compounds described as melting CPs, homogeneous melting processes were confirmed for their single crystals by observation with a microscope (Supporting Information Figure S1). The melting points of these compounds were determined on the basis of differential scanning calorimetry (DSC, Supporting Information Figure S2).

Figure 1. Photographs of **1**, **1′**, and **1″**.

These CPs are crystalline solids at 25 °C and become viscous liquids when heated to their melting points. Although the liquid states of these CPs more or less supercool due to their high viscosity, proper treatments for nucleation and crystal growth, such as mechanical milling, revert the materials to the original crystalline solids, as confirmed by PXRD measurements (Supporting Information Figure S3). Whereas **1** and **3** have one-dimensional (1D) coordination structures, **2** has a two-dimensional (2D) structure, and all of these CPs reversibly transform from solid to liquid regardless of the differences in the structural dimensionality (1D or 2D), coordination geometry (O_h or T_d), and coordination species (phosphate or 1,2,4-triazole).

We synthesized the following structures analogous to **3** with different organic moieties and metal centers to extract the key factors involved in melting: $[Zn_3(H_2PO_4)_6(H_2O)_3]\cdot H$(2-MeBim) (**4**; 2-MeBim: 2-methylbenzimidazolate), $[Zn_3(H_2PO_4)_6(H_2O)_3]\cdot H$(2-ClBim) (**5**; 2-ClBim: 2-chlorobenzimidazolate), and $[Co_3(H_2PO_4)_6(H_2O)_3]\cdot HBim$ (**6**). The

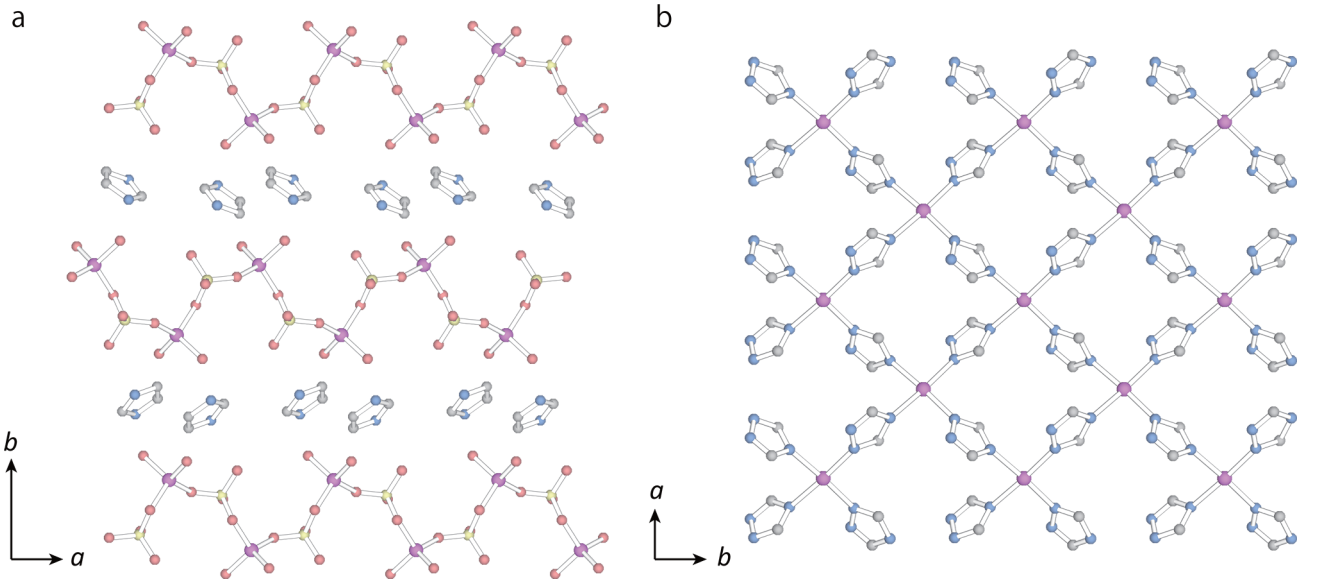

Figure 2. Crystal structures of (a) **1** and (b) **2**. The Zn, P, O, N, and C atoms are shown in purple, yellow, red, blue, and gray, respectively. Phosphates that do not bridge the zinc ions are not shown for the explicit visualization of the extended coordination structures; H atoms have been omitted.

DOI: 10.1021/ja511019u
J. Am. Chem. Soc. 2015, 137, 864–870

structural similarities with **3** were identified by single crystal structural analysis for **4** and via PXRD for **5** and **6** (Supporting Information Table S2, Figure S4). We observed the melting of **4** at 97 °C in the same manner as **3**; however, **5** solidifies just after the solid-to-liquid transition at approximately 100 °C, and **6** gradually decomposes without melting at over 200 °C. For **5**, the liquid form is not stable; for **6**, some components evaporate, and the processes are thus irreversible and not defined as melting. The diversity observed for **3**, **4**, **5**, and **6**, despite the structural similarity of these CPs, indicates that thermal behavior (melting or decomposition) is sensitive to slight alterations in chemical composition. The host–guest interaction strength or pK_a of the guest molecules may result in the differences for **4** and **5**, whereas the stronger coordination bond possibly prevents congruent melting for **6**.[16]

It is expected that one of the key factors for melting is the coexistence of phosphate and azoles in the structures because these moieties can form ion pairs by donating/accepting protons. The high ionicity of the compounds plays an important role in stabilizing the liquid state of these CPs, suppressing the partial vaporization of a component with Coulomb interactions, which work as effective cohesive forces in the liquid states. The fact that we did not observe melting for **5** or **6** indicates that the melting of phosphate-containing inorganic–organic hybrid materials (including organically templated metal phosphates) is not necessarily common.[17] Therefore, the CPs we reported here are built on a fine balance of composition, ionicity, and bond strength that affords the series of melting phenomena for CPs. Different from inorganic metal phosphates, the organic moieties and acidic hydrogen atoms remaining on the phosphate ligands in the melting CPs cause melting in a relatively low temperature range.

The CPs with slow recrystallization rates can form a glass (supercooled liquid that has lost its ability to flow[4a]) at ambient temperature, which is one of the advantageous aspects of these compounds. Of the melting CPs studied, **2″** is the slowest to recrystallize, and the glassy supercooled state is stable in a wide temperature range, whereas **3″** quickly recrystallizes when it is cooled to ambient temperature. In the case of **1**, the supercooled state is metastable at ambient temperature, whereas recrystallization is promoted at 100 °C. Because of the controllable nature of this CP, we selected **1** as a representative of the melting CPs to investigate the fundamental features of the melting behavior. Compared with molecular systems (including ionic liquids), the presence of a coordination center (zinc ion) is expected to feature in the melting, recrystallization, and glass formation of **1**.

Regarding the melting process of crystalline solids, Lindemann's rule empirically describes $f = u/d$, where u is the mean thermal atomic displacement (the square root of the Debye–Waller factor) of an atom, and d is the bond distance to the nearest-neighbor atom, which universally approaches 0.10 to 0.13 near the melting temperature.[18] On the basis of this rule, we analyzed the thermal vibrations of the oxygen atoms that coordinate to the zinc ion of **1** because one of the critical steps in melting is expected to be the dissociation of the coordination bonds (if any), which occurs with (or follows) the loosening of the close packing of the 1D zinc-phosphate chains. Of the four coordinating oxygen atoms, the O9 of one H_2PO_4 ligand (P3) displays a higher degree of vibration than the other oxygen atoms (Figure 3). The cause of this anomaly lies in the imidazolium cation of **1** with a high Debye–Waller factor, which is rotatable at high temperature.[12a] The P3 phosphate is

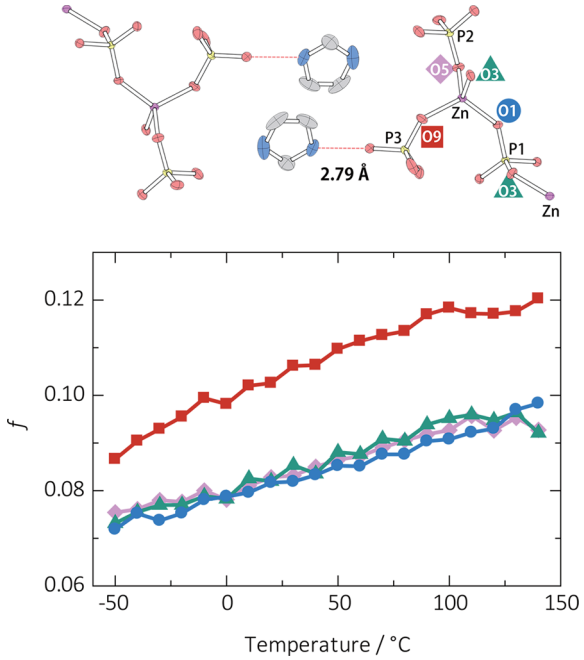

Figure 3. Degrees of the thermal vibrations of oxygen atoms around the zinc ion. O1 (blue circles), O3 (green triangles), O5 (purple diamonds), and O9 (red squares). The ORTEP model of **1** (at −50 °C) and the H-bond distances are shown on the top. The Zn, P, O, N, and C atoms are shown in purple, yellow, red, blue, and gray, respectively; H atoms have been omitted.

hydrogen-bonded with the rotatable imidazolium; therefore, O9 has a higher thermal factor. At 140 °C, just below the melting point of **1**, f(O9) is 0.12, while f(O1), f(O3), and f(O5) are less than 0.10, indicating that the bond dissociation between Zn–O9 triggers the melting of **1** by breaking the stable tetrahedral arrangement of the zinc ion, which is readily followed by the dissociation of the other Zn–O bonds. Thus, the organic moiety apparently plays an important role in the phase transition, inducing the melting process in **1**. The mobile imidazolium cations also loosen the packing of the zinc-phosphate chains because these cations occupy the interchain space in the crystal structure.

The atomic structures of CPs in liquid or glass states have rarely been discussed. One of the most intriguing aspects of this system is whether any coordination bonds are "preserved" in **1′** and **1″**. We use the term "preserved" to indicate the state in which coordination bonds are persistent without rapid breaking and re-forming events. For the structure of **1′**, the single crystal X-ray study discussed above implied that the coordination bonds are cleaved at the melting point. The solid-state ^{31}P NMR spectrum of **1′** at 160 °C, which shows a single sharp peak, is consistent with this interpretation and suggests that **1′** is an ionic liquid (discrete molecular fragments) of zinc, phosphate, and imidazolium ions without a preserved coordination bond, regardless of the strong bond-forming preference of zinc ions (Figure 4a). A dynamic mechanical analysis (DMA) of **1′** also supports the cleaved-bond model. The shear modulus of **1′** has a peak for G'' (the loss modulus) near 30 °C, which corresponds to the glass transition, and above that temperature, G'' remains higher than G' (the storage modulus) (Figure 4b). This profile is typical for viscoelastic fluids; there is a flow regime ($G'' > G'$) immediately after the glass transition. If there are coordination bonds (and, hence, a

DOI: 10.1021/ja511019u
J. Am. Chem. Soc. 2015, 137, 864–870

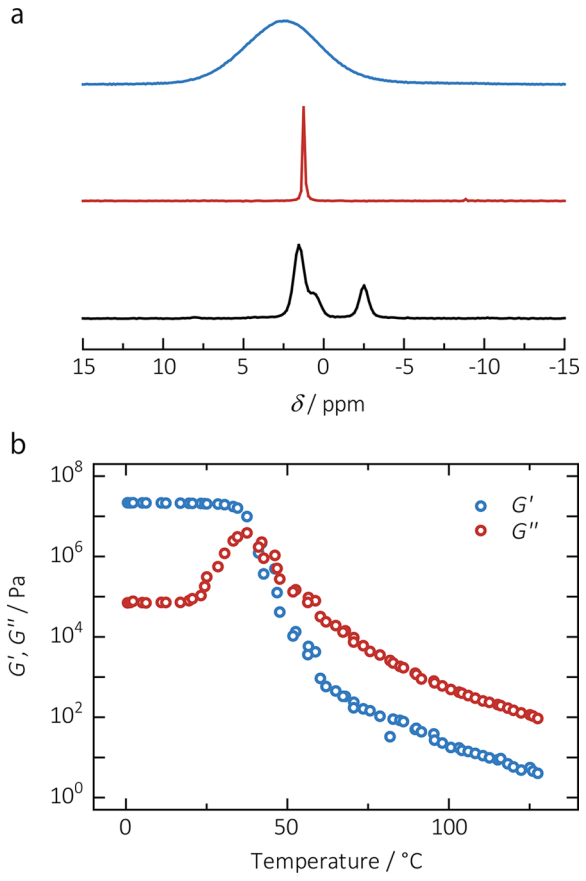

Figure 4. (a) Solid-state ^{31}P NMR spectra of **1** (black) at 25 °C, **1′** (red) at 160 °C, and **1″** (blue) at 5 °C. (b) Temperature-dispersive DMA from 0 °C (**1″**) to 130 °C (**1′**).

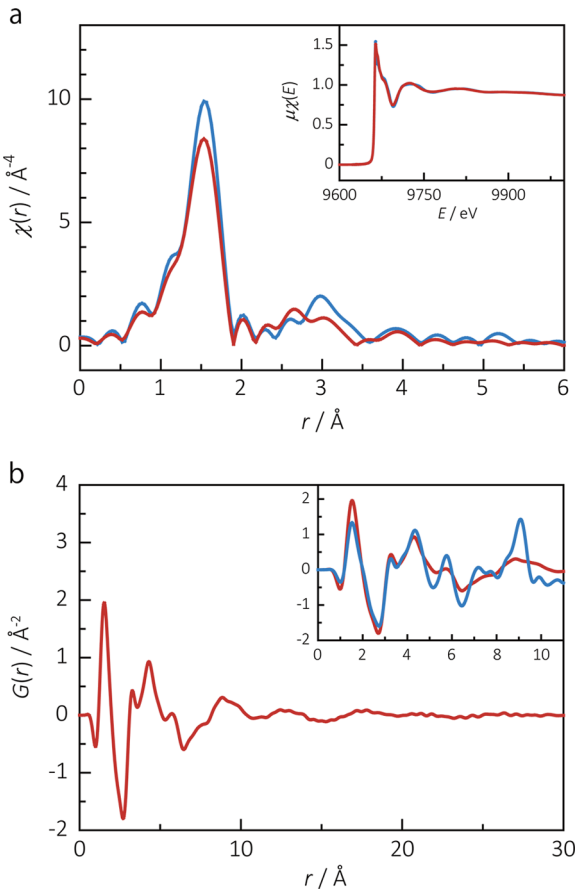

Figure 5. (a) The RDFs of **1** (blue) and **1″** (red) derived from the XASs (inset). (b) The PDF of **1″** (red), and the comparison of the short-range PDFs of **1** (blue) and **1″** (inset).

1D chained structure) preserved in **1′**, the effect of entangled chains should be present, as is often the case with linear organic polymers.[19] This phenomenon is represented as a rubbery plateau regime ($G' > G''$) after the glass transition, and the absence of a rubbery regime for **1′** is consistent with the cleaved-bond model.[20] The viscosity of **1′** deduced from the shear modulus has the typical profile for ionic liquids as well (Supporting Information Figure S5).

The solid-state ^{31}P NMR spectrum of **1″** at 5 °C is broader than **1′** that could not be fitted by a single Gaussian curve (Figure 4a). The spectrum indicates that the phosphates of **1″** are in various chemical environments, and some possibly coordinate to zinc ions. The IR spectrum of **1″** shows an N−H stretching band that is almost identical to that of crystalline **1** (Supporting Information Figure S6), suggesting that the imidazole molecules remain protonated (H_2Im^+) and do not coordinate to the zinc ions in **1″**. For an exact determination of the coordination environment of the zinc ions in **1″**, we measured the X-ray absorption spectrum (XAS) of the zinc ion of **1″**. The radial distribution functions (RDFs) around the zinc ions of **1** and **1″** deduced from their XASs indicate that the first coordination spheres of the zinc ions of **1** and **1″** are qualitatively identical (Figure 5a). The RDF of **1″** is fitted well by a model in which the zinc ions are surrounded by four oxygen atoms that have approximately the same Zn−O bond distance as **1** (Supporting Information Figure S7, Table S3). Because the molar ratio of zinc ion to phosphate ligand of **1″** is 1:3, one of the three phosphates coordinates to the zinc ion with two oxygen atoms (and the other phosphates coordinate to the zinc ion with one oxygen atom) to satisfy the four-coordinate requirement, which indicates that one phosphate bridges two zinc ions. This analysis illustrates the 1D polymeric structure of **1″** that is similar to that of **1**.

The pair distribution function (PDF) obtained from X-ray total scattering measurements revealed the structure of **1″** on a longer length scale (Figure 5b, Supporting Information Figure S8). The notable feature of the PDF of **1″** is the presence of four clear peaks below 6 Å, the positions of which are virtually identical to those in the PDF of **1**, although the third and fourth peaks of **1″** are broader. The fourth peak at 5.7 Å, which corresponds to the Zn−Zn distance observed in the crystal structure of **1**, indicates that the distance between two zinc ions is relatively fixed and that some degree of order persists within this region. This result compatibly supports the 1D chained model of **1″** suggested by the XAS in which the phosphates bridge two zinc ions. The PDF of **1″** becomes broader at approximately $r = 10$ Å and nearly featureless at $r > 20$ Å. Thus, the order limit of **1″** is the distance between two neighboring zinc ions, exhibiting characteristics similar to amorphous zeolitic imidazolate frameworks (*a*-ZIFs) that feature two metal ions bridged by one imidazolate ligand.[21]

A schematic illustration of the structures of **1**, **1′**, and **1″** is given in the Supporting Information (Figure S9). In the case of *a*-ZIFs, coordination bonds are preserved after the amorphization, thereby exemplifying a solid-to-solid transition. Due to the bond cleavage during the transition from **1** to **1′**, **1′** has sufficient fluidity to be regarded as a liquid; thus, the transition

DOI: 10.1021/ja511019u
J. Am. Chem. Soc. 2015, 137, 864−870

is observed as solid-to-liquid instead of solid-to-solid. Compared to the amorphization, important advantages of the melting frameworks are the processing and shaping ability via the liquid states that enable recrystallization and grain-boundary-free fabrications.

To demonstrate the utility of the phase transition of CPs, we fabricated a thin film of **1** and aligned the orientations of the crystals of **1** on a glass substrate through a simple melting and recrystallization process. The crystals of **1** grown from **1′** pressed between two ITO glasses at 100 °C (the crystallization temperature for **1′**) formed a thin film with a thickness of 8 μm. The film crystals were observed with a microscope, and the radial crystal growth of **1** was confirmed (Figure 6a). The

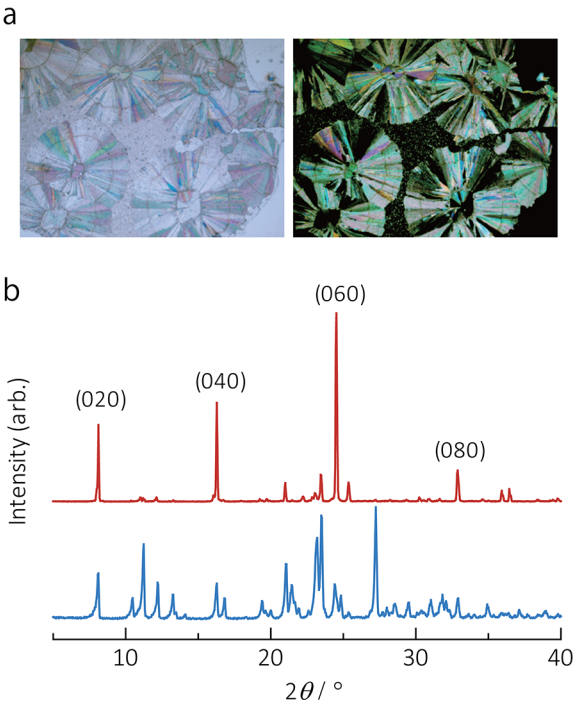

Figure 6. (a) Microscopy images (top view) of the spherulites of **1** (left) and **1** with polarized light (right). (b) The XRD pattern of the spherulites of **1** (red) compared with the powder of **1** (blue).

observed morphology is known as spherulites, a typical morphology for crystals of nonbranched linear organic polymers.[22] PXRD of the spherulites of **1** reveals dominant peaks for the 0*k*0 Bragg diffractions, which indicates that the crystals are aligned such that the {010} lattice planes are preferentially oriented parallel to the glass plate (Figure 6b). Accordingly, [100], which is normal to [010], radially extends in the plate to form spherulites, reflecting the 1D structure of **1**, in which the coordination chains are in the [100] direction.

Because **1** is a proton-conductive CP, the reduced thickness leads to a reduced resistivity regarding proton conduction. The temperature-dependent resistivity of the thin film of **1** was measured via AC impedance under anhydrous conditions. The fitting of the Nyquist plot at 70 °C with an equivalent circuit revealed a resistance of 115 Ω (Figure 7a), which is 480 times lower than the resistivity of the pellet of recrystallized **1** (thickness of 1.05 mm) fabricated by pressing the powder crystals of **1**.[12a] The resistivity reached 28 Ω at a minimum at 120 °C, demonstrating improved performance due to flexible processability (Supporting Information Figure S10).

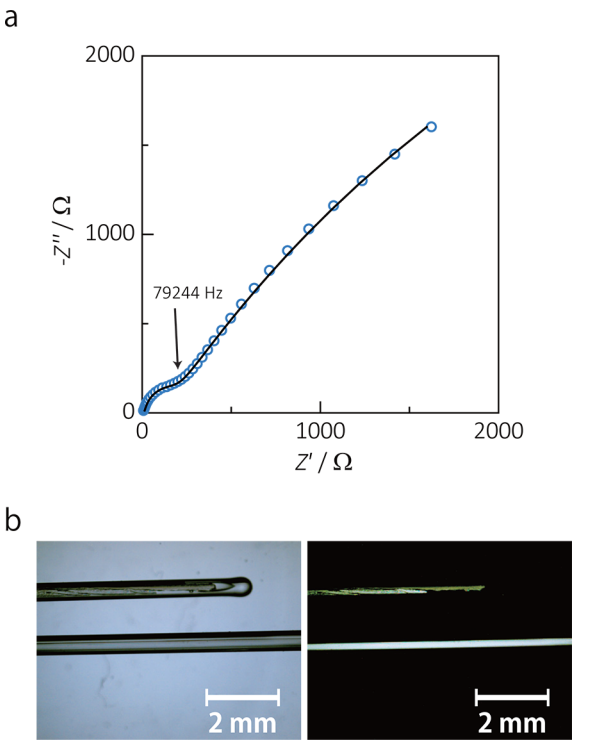

Figure 7. (a) A Nyquist plot of the thin film of **1** at 70 °C (left). Blue circles are the experimental data, and the black line shows simulated values from an equivalent circuit. (b) Microscopy images of the monolith crystal of **1** (left) and **1** with polarized light (right) in a glass capillary.

We also fabricated a monolith crystal of **1** in a capillary with the melt growth technique. We employed a Bridgeman-like method as follows: **1** was placed in a glass capillary and melted; **1′**, which filled the capillary, was then slowly crystallized in a thermal gradient. The obtained single crystal was 0.2 mm in thickness and more than 1 cm in length (Figure 7b). Thus, a crack-free monolith crystal of **1** can be grown, even in a narrow space, which is not possible with conventional crystallization methods of CPs, such as solvothermal reactions.

■ CONCLUSIONS

Unlike most substances (such as organics, inorganics, and polymers), the reversible solid−liquid phase transition of inorganic−organic hybrid materials has not been taken for granted. In this report, we have synthesized and investigated a class of CPs from the perspective of the solid−liquid phase transition of hybrid materials and found that a balance of high ionicity and coordination bond strength in the composition is critical for a reversible solid−liquid phase transition. As inorganic−organic hybrid materials, the organic moiety of the CPs triggers the initial step of melting. With regard to the behavior of the main cohesive forces of CPs, coordination bonds, the liquid state is fluid without preserving coordination bonds, in which Coulomb interactions may become more important, whereas the glassy state has a polymeric structure with re-formed coordination bonds. Recrystallization from the liquid state provides a facile fabrication method for thin films, the alignment of crystal orientation, and the growth of a monolith crystal. The methods demonstrated in this study have not been available for conventional hybrid materials including CPs, which commonly decompose irreversibly when heated.

DOI: 10.1021/ja511019u
J. Am. Chem. Soc. 2015, 137, 864−870

We expect that the glass formation, shaping, and melt growth process for the crystals of CPs demonstrated here can be extended to various crystalline hybrid materials, which will lead to a useful strategy for synthesizing and processing inorganic–organic hybrid materials in future. Study of the pressure effect on melting hybrid materials through examination of the phase diagrams should be a next challenge.

EXPERIMENTAL SECTION

Materials. All reagents and chemicals were obtained from commercial sources, of reagent grade, and used without further purification. The CPs, $[Zn(HPO_4)(H_2PO_4)_2]\cdot 2H_2Im$ (**1**), $[Zn(H_2PO_4)_2(HTr)_2]$ (**2**), and $[Zn_3(H_2PO_4)_6(H_2O)_3]\cdot HBim$ (**3**), were prepared using previously described methods.[12a,14,15]

*Synthesis of $[Zn_3(H_2PO_4)_6(H_2O)_3]\cdot H(2\text{-}MeBim)$ (**4**) and $[Zn_3(H_2PO_4)_6(H_2O)_3]\cdot H(2\text{-}ClBim)$ (**5**).* Zinc oxide (243 mg, 3 mmol), 2-methylbenzimidazole (132 mg, 1 mmol), and phosphoric acid (85% in H_2O, 402 μL, 6 mmol) were placed in a 10 mL Teflon jar with two steel-cored 10 mm Teflon balls. The mixture was ground for 60 min in a Retch MM200 grinder mill operating at 25 Hz. The powder obtained was washed with methanol and evacuated at ambient temperature overnight to yield dry **4** in pure phase. The same procedure was applied for **5**, using 2-chlorobenzimidazole (153 mg, 1 mmol) instead of 2-methylbenzimidazole.

*Synthesis of $[Co_3(H_2PO_4)_6(H_2O)_3]\cdot HBim$ (**6**).* Cobalt oxide (224 mg, 3 mmol), benzimidazole (132 mg, 1 mmol), phosphoric acid (85% in H_2O, 402 μL, 6 mmol) were placed in a 10 mL Teflon jar with two steel-cored 10 mm Teflon balls. The mixture was ground for 30 min in a Retch MM200 grinder mill operating at 25 Hz. The mixture was placed in a glass vial, which was then tightly capped and heated at 120 °C in an oven for 2 days. The powder obtained was washed with ethanol and filtered to yield **6** in pure phase.

X-ray Characterization. The synchrotron X-ray absorption spectra and total scattering for **1** and **1″** were collected at the Aichi Synchrotron Radiation Center (Aichi SR) on beamlines BL5S1 and BL5S2, respectively. X-ray absorption spectra in the energy region of the Zn K-edge were measured in transmission mode with a Si(111) double-crystal monochromator and ion chambers and processed using the IFEFFIT library.[23] Fourier transformation was $k3$-weighted in the k range from 3.0 to 13.0 Å^{-1}. The X-ray total scattering data were collected at λ = 0.62 Å with a large Debye–Scherrer camera and imaging plate covering the Q range from 0.3 to 14.8 Å^{-1}. The correction of the data for Compton scattering, multiplicative contributions, and Fourier transformation were performed with PDFgetX3.[24] A Gauss window ($\exp[-BQ^2]$, B = 0.023) was applied before converting the structure functions into PDFs to suppress truncation errors.

Conductivity Measurements. The impedance spectra of the thin film of **1** from 30 °C to 120 °C were measured using an impedance and gain-phase analyzer (Solartron SI 1260) over the frequency range 1 Hz to 5 MHz with an input voltage amplitude of 30 mV. The impedance cell was filled with dry N_2 at atmospheric pressure. The measurements were performed at thermal equilibrium by holding for 30 min at each measuring temperature. ZView software was used to fit the impedance data sets by means of an equivalent circuit simulation to obtain the resistance values.

ASSOCIATED CONTENT

Supporting Information

Experimental details, microscopy images, PXRD, crystal data, viscosity measurement, IR, RDF fitting, X-ray total scattering, Nyquist plot, tables, and schemes. This material is available free of charge via the Internet at http://pubs.acs.org.

AUTHOR INFORMATION

Corresponding Authors

horike@sbchem.kyoto-u.ac.jp

kitagawa@icems.kyoto-u.ac.jp

Notes

The authors declare no competing financial interest.

ACKNOWLEDGMENTS

This work was supported by the PRESTO of the Japan Science and Technology Agency (JST), and a Grant-in-Aid for Scientific Research on the Innovative Areas: “Fusion Materials”, and Grant-in-Aid for Young Scientists (A) from the Ministry of Education, Culture, Sports, Science and Technology, Japan. iCeMS is supported by the World Premier International Research Initiative (WPI) of MEXT, Japan. D.U. is grateful to JSPS Research Fellowships for Young Scientists. The authors thank Dr. Takashi Fukuda (Osaka University), Dr. Kazunori Sato (Osaka University), and Dr. Makoto Negoro (Osaka University) for technical advice on the Bridgeman crystal growth. The authors thank Dr. Yuh Hijikata (Nagoya University) and Dr. Tomohiro Fukushima (Massachusetts Institute of Technology) for helpful discussion.

REFERENCES

(1) (a) Atkins, P.; De Paula, J. *Physical Chemistry*; Oxford University Press: Cary, NC, 2006. (b) Mochizuki, K.; Matsumoto, M.; Ohmine, I. *Nature* **2013**, *498*, 350.

(2) (a) Pamplin, B. R. *Crystal Growth*; Pergamon Press: New York, 1975. (b) Yasuda, H.; Ohnaka, I.; Yamamoto, Y.; Wismogroho, A. S.; Takezawa, N.; Kishio, K. *Mater. Trans.* **2003**, *44*, 2550. (c) Liu, Y. C.; Deal, M. D.; Plummer, J. D. *J. Electrochem. Soc.* **2005**, *152*, G688.

(3) (a) Matthias, B. T.; Remeika, J. P. *Phys. Rev.* **1949**, *76*, 1886. (b) Keck, P. H.; Golay, M. J. E. *Phys. Rev.* **1953**, *89*, 1297. (c) Heath, J. R. *Science* **1992**, *258*, 1131.

(4) (a) Angell, C. A. *Science* **1995**, *267*, 1924. (b) Shopsowitz, K. E.; Qi, H.; Hamad, W. Y.; MacLachlan, M. J. *Nature* **2010**, *468*, 422.

(5) (a) Cox, P. A. *The Electronic Structure and Chemistry of Solids*; Oxford University Press: Cary, NC, 1987. (b) Israelachvili, J. N. *Intermolecular and Surface Forces*, 2nd ed.; Academic Press: New York, 1992.

(6) (a) Rao, C. N. R.; Natarajan, S.; Vaidhyanathan, R. *Angew. Chem., Int. Ed.* **2004**, *43*, 1466. (b) Sanchez, C.; Julian, B.; Belleville, P.; Popall, M. *J. Mater. Chem.* **2005**, *15*, 3559. (c) Cheetham, A. K.; Rao, C. N. R.; Feller, R. K. *Chem. Commun.* **2006**, 4780. (d) Hoffmann, F.; Cornelius, M.; Morell, J.; Fröba, M. *Angew. Chem., Int. Ed.* **2006**, *45*, 3216.

(7) (a) Donaruma, L. G.; Block, B. P.; Loening, K. L.; Plate, N.; Tsuruta, T.; Buschbeck, K. C.; Powell, W. H.; Reedijk, J. *Pure Appl. Chem.* **1985**, *57*, 149. (b) Moulton, B.; Zaworotko, M. J. *Chem. Rev.* **2001**, *101*, 1629. (c) Carlucci, L.; Ciani, G.; Proserpio, D. M. *Coord. Chem. Rev.* **2003**, *246*, 247. (d) Janiak, C. *Dalton Trans.* **2003**, 2781. (e) Batten, S. R.; Champness, N. R.; Chen, X.-M.; Garcia-Martinez, J.; Kitagawa, S.; Ohrstrom, L.; O'Keeffe, M.; Suh, M. P.; Reedijk, J. *CrystEngComm* **2012**, *14*, 3001.

(8) (a) Pei, Y.; Verdaguer, M.; Kahn, O.; Sletten, J.; Renard, J. P. *J. Am. Chem. Soc.* **1986**, *108*, 7428. (b) Batten, S. R.; Murray, K. S. *Coord. Chem. Rev.* **2003**, *246*, 103.

(9) Kishida, H.; Matsuzaki, H.; Okamoto, H.; Manabe, T.; Yamashita, M.; Taguchi, Y.; Tokura, Y. *Nature* **2000**, *405*, 929.

(10) (a) Kitagawa, H.; Onodera, N.; Sonoyama, T.; Yamamoto, M.; Fukawa, T.; Mitani, T.; Seto, M.; Maeda, Y. *J. Am. Chem. Soc.* **1999**, *121*, 10068. (b) Nagao, Y.; Fujishima, M.; Ikeda, R.; Kanda, S.; Kitagawa, H. *Inorg. Chem. Commun.* **2003**, *6*, 346. (c) Ballesteros-Rivas, M.; Ota, A.; Reinheimer, E.; Prosvirin, A.; Valdés-Martinez, J.; Dunbar, K. R. *Angew. Chem.* **2011**, *123*, 9877.

(11) (a) Yaghi, O. M.; O'Keeffe, M.; Ockwig, N. W.; Chae, H. K.; Eddaoudi, M.; Kim, J. *Nature* **2003**, *423*, 705. (b) Kitagawa, S.; Kitaura, R.; Noro, S. *Angew. Chem., Int. Ed.* **2004**, *43*, 2334. (c) Kepert, C. J. *Chem. Commun.* **2006**, 695. (d) Ferey, G. *Chem. Soc. Rev.* **2008**,

DOI: 10.1021/ja511019u
J. Am. Chem. Soc. 2015, 137, 864–870

37, 191. (e) Hurd, J. A.; Vaidhyanathan, R.; Thangadurai, V.; Ratcliffe, C. I.; Moudrakovski, I. L.; Shimizu, G. K. *Nat. Chem.* **2009**, *1*, 705. (f) Murray, L. J.; Dinca, M.; Long, J. R. *Chem. Soc. Rev.* **2009**, *38*, 1294.
(12) (a) Horike, S.; Umeyama, D.; Inukai, M.; Itakura, T.; Kitagawa, S. *J. Am. Chem. Soc.* **2012**, *134*, 7612. (b) Eike, T. S.; Edengeiser, E.; Mallick, B.; Havenith, M.; Mudring, A.-V. *Chem.—Eur. J.* **2014**, *20*, 5338.
(13) (a) Zacher, D.; Shekhah, O.; Woll, C.; Fischer, R. A. *Chem. Soc. Rev.* **2009**, *38*, 1418. (b) Talin, A. A.; Centrone, A.; Ford, A. C.; Foster, M. E.; Stavila, V.; Haney, P.; Kinney, R. A.; Szalai, V.; El Gabaly, F.; Yoon, H. P.; Léonard, F.; Allendorf, M. D. *Science* **2014**, *343*, 66.
(14) Umeyama, D.; Horike, S.; Inukai, M.; Itakura, T.; Kitagawa, S. *J. Am. Chem. Soc.* **2012**, *134*, 12780.
(15) Umeyama, D.; Horike, S.; Inukai, M.; Kitagawa, S. *J. Am. Chem. Soc.* **2013**, *135*, 11345.
(16) (a) Shriver, D. F.; Atkins, P. *Inorganic Chemistry*; Oxford University Press: Cary, NC, 1999. (b) Tan, J.-C.; Jain, P.; Cheetham, A. K. *Dalton Trans.* **2012**, *41*, 3949.
(17) (a) Alberti, G.; Casciola, M.; Costantino, U.; Vivani, R. *Adv. Mater.* **1996**, *8*, 291. (b) Cheetham, A. K.; Ferey, G.; Loiseau, T. *Angew. Chem., Int. Ed.* **1999**, *38*, 3268. (c) Rao, C. N. R.; Natarajan, S.; Neeraj, S. *J. Am. Chem. Soc.* **2000**, *122*, 2810. (d) Clearfield, A.; Wang, Z. K. *J. Chem. Soc., Dalton Trans.* **2002**, 2937. (e) Cooper, E. R.; Andrews, C. D.; Wheatley, P. S.; Webb, P. B.; Wormald, P.; Morris, R. E. *Nature* **2004**, *430*, 1012. (f) Fan, J.; Hanson, B. E. *Inorg. Chem.* **2005**, *44*, 6998.
(18) (a) Lindemann, F. A. *Phys. Z.* **1910**, *11*, 609. (b) Mei, Q. S.; Lu, K. *Prog. Mater. Sci.* **2007**, *52*, 1175.
(19) Colby, R. H.; Fetters, L. J.; Graessley, W. W. *Macromolecules* **1987**, *20*, 2226.
(20) John, M. D.; Ronald, G. L. *Structure and Rheology of Molten Polymers*; Carl Hanser Verlag GmbH & Co., KG: Munich, 2006.
(21) (a) Bennett, T. D.; Goodwin, A. L.; Dove, M. T.; Keen, D. A.; Tucker, M. G.; Barney, E. R.; Soper, A. K.; Bithell, E. G.; Tan, J.-C.; Cheetham, A. K. *Phys. Rev. Lett.* **2010**, *104*, 115503. (b) Bennett, T. D.; Keen, D. A.; Tan, J. C.; Barney, E. R.; Goodwin, A. L.; Cheetham, A. K. *Angew. Chem., Int. Ed.* **2011**, *50*, 3067. (c) Cairns, A. B.; Goodwin, A. L. *Chem. Soc. Rev.* **2013**, *42*, 4881. (d) Bennett, T. D.; Cheetham, A. K. *Acc. Chem. Res.* **2014**, *47*, 1555−1562.
(22) (a) Keller, A. *J. Polym. Sci.* **1955**, *17*, 291. (b) Ho, R.-M.; Ke, K.-Z.; Chen, M. *Macromolecules* **2000**, *33*, 7529.
(23) Ravel, B.; Newville, M. *J. Synchrotron Radiat.* **2005**, *12*, 537.
(24) Juhas, P.; Davis, T.; Farrow, C. L.; Billinge, S. J. L. *J. Appl. Crystallogr.* **2013**, *46*, 560.

DOI: 10.1021/ja511019u
J. Am. Chem. Soc. 2015, 137, 864−870